Real-time lumbosacral joint loading estimation in exoskeleton-assisted lifting conditions via electromyography-driven musculoskeletal models

Moya-Esteban, A.; Durandau, G.; van der Kooij, H.; Sartori, M.

DOI
10.1016/j.jbiomech.2023.111727

Publication date
2023

Document Version
Final published version

Published in
Journal of Biomechanics

Journal of Biomechanics 157 (2023) 111727

Contents lists available at ScienceDirect

Journal of Biomechanics

journal homepage: www.elsevier.com/locate/jbiomech

Real-time lumbosacral joint loading estimation in exoskeleton-assisted lifting conditions via electromyography-driven musculoskeletal models

A. Moya-Esteban [a,*], G. Durandau [a], H. van der Kooij [a,b], M. Sartori [a]

[a] Department of Biomechanical Engineering, University of Twente, Enschede, The Netherlands
[b] Department of Biomechanical Engineering, Delft University of Technology, Delft, The Netherlands

ARTICLE INFO

Keywords:
EMG-driven musculoskeletal modelling
Real-time
Back-support exoskeleton
Lumbosacral compression forces

ABSTRACT

Lumbar joint compression forces have been linked to the development of chronic low back pain, which is specially present in occupational environments. Offline methodologies for lumbosacral joint compression force estimation are not commonly integrated in occupational or medical applications due to the highly time-consuming and complex post-processing procedures. Hence, applications such as real-time adjustment of assistive devices (*i.e.,* back-support exoskeletons) for optimal modulation of compression forces remains unfeasible. Here, we present a real-time electromyography (EMG)-driven musculoskeletal model, capable of estimating accurate lumbosacral joint moments and plausible compression forces. Ten participants performed box-lifting tasks (5 and 15 kg) with and without the Laevo Flex back-support exoskeleton using squat and stoop lifting techniques. Lumbosacral kinematics and EMGs from abdominal and thoracolumbar muscles were used to drive, in real-time, subject-specific EMG-driven models, and estimate lumbosacral joint moments and compression forces. Real-time EMG-model derived moments showed high correlations (R^2 = 0.76 - 0.83) and estimation errors below 30% with respect to reference inverse dynamic moments. Compared to unassisted lifting conditions, exoskeleton liftings showed mean lumbosacral joint moments and compression forces reductions of 11.9 - 18.7 Nm (6 - 12% of peak moment) and 300 - 450 N (5 - 10%), respectively. Our modelling framework was capable of estimating in real-time, valid lumbosacral joint moments and compression forces in line with *in vivo* experimental data, as well as detecting the biomechanical effects of a passive back-support exoskeleton. Our presented technology may lead to a new class of bio-protective robots in which personalized assistance profiles are provided based on subject-specific musculoskeletal variables.

1. Introduction

Approximately 85% of the population will experience low back pain (LBP) at some point of their life (Freburger et al., 2009). Previous research has linked the onset of LBP to cumulative compression forces on the lumbar spine (Norman et al., 1998). Specifically, compression forces are associated to injury of joint surfaces, bone and soft tissues. Furthermore, compression forces contribute to reduction of intervertebral disc height and changes in apophyseal joint position, which may lead to chronic pain (Brinckmann et al., 1987).

LBP is specially present in occupational environments where heavy object handling and non-ergonomic postures are common (Ning et al., 2014). Passive back-support exoskeletons have shown the potential to reduce lumbar compression forces during heavy object lifting (Koopman et al., 2020a,b). Therefore, these exoskeletons have been introduced in occupational scenarios with the goal of relieving the load on the lower back of workers (Hensel and Keil, 2019; Settembre et al., 2020). Nonetheless, previous methodologies used to evaluate exoskeleton modulations on spinal compression forces relied on offline analyses, which cannot provide real-time biofeedback of such property. Hence, onsite personalization of exoskeletons to ensure optimal lumbar protection remains unfeasible.

Lumbar compression forces have been previously estimated by multiplying intervertebral disc areas by readings of intradiscal pressure sensors implanted in participants' spines (Schultz et al., 1982; Nachemson and Morris, 1964). Alternatively, compression forces can be directly measured by instrumented vertebral body replacements (Rohlmann et al., 1999, 2013). Nonetheless, due to the invasiveness and complexity of these methodologies as well as the scarcity of participants, non-invasive computational musculoskeletal modelling approaches have been regarded as a valuable alternative for spinal forces estimation (Dreischarf et al., 2016).

Computational neuromusculoskeletal models representing spinal anatomy and neuromechanics generally estimate trunk muscle forces,

* Corresponding author.
E-mail address: a.moyaesteban@utwente.nl (A. Moya-Esteban).

https://doi.org/10.1016/j.jbiomech.2023.111727
Accepted 14 July 2023
Available online 18 July 2023

Nomenclature

EMD	Electromechanical delay
EMG	Electromyography
ID	Inverse dynamics
IK	Inverse kinematics
IL	Iliocostalis
JRA	Joint reaction analysis
LBP	Low back pain
LFB	Lifting full body
LTpL	Longissimus thoracis pars lumborum
LTpT	Longissimus thoracis pars thoracis
MTU	Muscle tendon unit
RMSE	Root mean squared error
$RMSE_{BW}$	Root mean squared error normalized to body weight
$RMSE_{RMS}$	Root mean squared error normalized to root mean square of the reference moment

which are subsequently utilized to calculate spinal forces based on 3D geometrical models. Optimization-driven models estimate muscle forces based on one or more cost functions which aim at satisfying physiological assumptions, such as minimization of muscular activation (Kim and Zhang, 2017; Bassani et al., 2017) or stress (Bazrgari et al., 2007). However, these methodologies neglect antagonistic co-contraction (El Ouaaid et al., 2013), hence negatively impacting estimation accuracy. Alternatively, electromyography (EMG)-driven musculoskeletal modelling approaches use experimentally measured muscle activity and, altogether with computational formulations of muscle activation and contraction dynamics, allow for the estimation of compression forces (Van Dieen and Kingma, 2005; Moya-Esteban et al., 2022; Hughes et al., 1994). Nonetheless, previously validated offline models require complex post-processing analyses, hampering their translation to clinical and occupational applications.

Real-time methodologies offer the advantage of estimating biomechanical properties with no post-processing steps and the subsequent time-delay, therefore providing numerous applications including personalized clinical (Pizzolato et al., 2017b) or ergonomic (Boocock et al., 2019) biofeedback, as well as control of assistive devices such as actuated exoskeletons (Durandau et al., 2022; Lu et al., 2017), where the estimated variable can be used to determine the onset and magnitude of the assistance. Previous studies have proposed tools for real-time lumbar compression forces estimation. However, these were static optimization-based approaches (Ventura et al., 2021; Samy et al., 2019) or lacked a detailed representation of musculoskeletal geometries or EMG-to-activation physiological processes (Peters et al., 2022; Fortini et al., 2020; Lorenzini et al., 2022), thus, hampering estimation accuracy and ultimately, their applicability to real-world scenarios.

Although previous authors have presented detailed and physiologically-correct real-time EMG-driven musculoskeletal models for moment estimation of the knee (Durandau et al., 2017, 2022), ankle (Manal et al., 2012), elbow (Lotti et al., 2020), wrist (Sartori et al., 2018) and contact forces at the knee (Pizzolato et al., 2017b), to the best of our knowledge, this is the first study to provide and validate an EMG-driven musculoskeletal model of the trunk, capable of estimating lumbosacral joint moments and compression forces in real-time. Additionally, for the first time, we employed our proposed methodology to evaluate in real-time the biomechanical effects of a passive back-support exoskeleton on thoracolumbar muscle activity, lumbosacral joint moments and compression forces. This study constitutes the first step for the development of real-time and non-invasive technologies capable of quantifying the bio-protective effect of assistive devices. This is central for lumbar loading biofeedback and robotic control technologies, which may have a significant impact in real-world applications for preventing musculoskeletal disorders, including clinical, rehabilitation, robotic, occupational and sports-related.

Fig. 1. Participant wearing the back-support Laevo Flex exoskeleton. The exoskeleton is a passive device which transfers loads from the lower back to the chest and thighs. The delivered assistance is provided by spring-like mechanisms acting around the trochanter major (hip joint). Spring mechanisms store energy in the bending down phase of the movement, which is (partially, as a result of hysteresis) returned to the user in the lifting phase. The smaller the torso-thigh angle, the higher the moment produced by the exoskeleton. The actuator strength was set to 70% (medium assistance) for all participants and lifting conditions.

2. Methods

2.1. Subjects and apparatus

The experimental procedure was approved by the Natural Sciences and Engineering Sciences Ethics committee of the University of Twente (reference: 2022.175). Ten participants (4 female; age: 28 ± 3, height: 173 ± 7 cm, weight: 67 ± 9 kg) with no history of LBP participated in the study after giving written informed consent.

Participants performed box-lifting tasks (Section 2.3) with and without the Laevo Flex exoskeleton (Laevo, Rijswijk, The Netherlands, see Fig. 1). The spring actuator strength of the exoskeleton was set to 70% (medium strength), providing an average extension assistance moment of 25 N m (peak moment: 41 N m) at hip joint level (van Harmelen et al., 2022). A twelve-camera Qualisys system (Qualisys Medical AB, Sweden) recorded and labelled in real-time the 3D trajectories of 33 reflective markers (32 on the participant and 1 on the upper edge of the lifted box) at 15 Hz. Markers were placed on participants' upper limbs, trunk and pelvis as described in Moya-Esteban et al. (2020). Surface EMGs from rectus abdominis (umbilicus level), iliocostalis (IL, 6 cm lateral to L2), longissimus thoracis pars lumborum (LTpL, 3 cm lateral to L1) and pars thoracis (LTpT, 4 cm lateral to T10) muscles were recorded using Ottobock 13E400 electrodes (Ottobock SE&Co. KGaA, Duderstadt, Germany) at 1000 Hz. Electrode placement was earlier reported in Moya-Esteban et al. (2022).

The real-time software was executed on a Lenovo ThinkStation P620 (AMD Ryzen Threadripper PRO 3975WX, 3.50 GHz, 32 cores, 64 threads, 128 GB of RAM, and Windows 10).

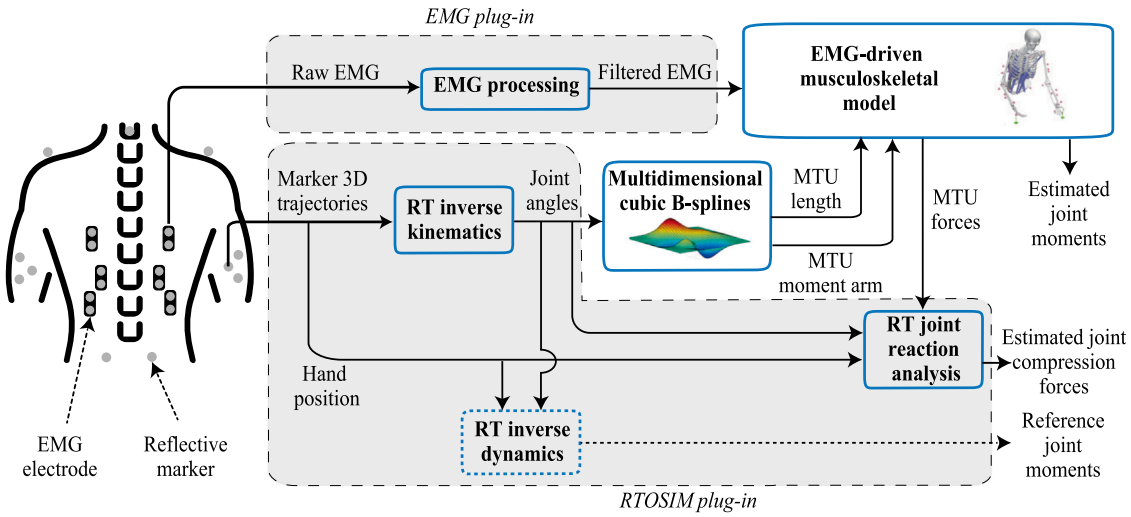

Fig. 2. Schematic representation of real-time (RT) EMG-driven musculoskeletal modelling framework including: (1) motion capture (Qualisys) and EMG measuring systems, (2) two plug-ins (RTOSIM and EMG) provide an interface between measuring devices and EMG-driven musculoskeletal model, as well as manage the data processing, (3) a multidimensional cubic B-spline block which enables real-time performance by computing muscle–tendon unit (MTU)-specific lengths and three-dimensional moment arms using L5/S1 joint angles as input (Sartori et al., 2012a) and (4) our previously validated EMG-driven musculoskeletal modelling framework, which includes a representation of MTU activation and force generation dynamics (Moya-Esteban et al., 2022; Pizzolato et al., 2015). The components of the pipeline exclusively used for model calibration and validation are indicated with dotted lines.

2.2. Real-time pipeline

Based on our previously developed real-time modelling pipeline (Durandau et al., 2017) and our validated EMG-driven musculoskeletal model for lumbosacral joint (L5/S1) compression force estimation (Moya-Esteban et al., 2022), we developed a C++ framework which takes EMGs and L5/S1 joint kinematics as input, and estimates L5/S1 flexion-extension moments and compression forces in real-time. The structure of this real-time modelling framework is depicted in Fig. 2. In our framework, two plug-ins manage the connection between measurement devices, OpenSim API (Delp et al., 2007) and EMG-driven musculoskeletal model, as well as the data processing (Section 2.2.2).

2.2.1. Anatomical model

The OpenSim lifting full-body (LFB) model (Beaucage-Gauvreau et al., 2019) was used to compute real-time L5/S1 joint moments via inverse dynamics (ID) methodology. ID moments were used to calibrate the EMG-driven model (see Section 2.2.3) as well as reference moments for validation purposes. To achieve real-time performance, a series of modifications were applied to the base LFB model (see Table 1). In the original LFB model, kinematic coupler constraints prescribed the angle of lumbar vertebrae as a function of L5/S1 joint angles. However, the use of such constraints is discouraged for real-time applications due to the increased inverse kinematics computation time, resulting from the added complexity to the model (Sherman et al., 2011). Therefore, we deactivated all kinematic coupler constrains present in the lifting full-body model. Given that we used a top-bottom approach for the estimation of lumbo-sacral joint inverse dynamics moments, we removed thighs, shanks and feet from the model, reducing the number of model bodies and degrees of freedom. Due to the negligible wrist movement in our experimental protocol, wrist joints were welded, thus, not allowing any translation or rotation. As our main goal consists of the computation of L5/S1 flexion-extension joint moments and compression forces, muscle–tendon units (MTU) with no mechanical effect around such degree of freedom were eliminated.

2.2.2. Plug-ins

Qualisys software automatically identified and labelled 3D marker trajectories, which were received by the real-time OpenSim, RTOSIM plug-in Pizzolato et al. (2017a), via TCP/IP. OpenSim API used then marker trajectories to perform inverse kinematics (IK) and ID, using the adapted LFB model (scaled to participants' anthropometry). To achieve real-time performance, a multi-threading approach enabled the parallelization of six simultaneous IK optimizations (Pizzolato et al., 2017a). To calculate reference ID moments (used for EMG-model calibration and validation), we estimated the forces originating from the known weight of the lifted boxes. The Y-position of the marker placed on the box was compared to its resting Y-position (threshold) when the box was not being lifted. Whenever the box marker exceeded the threshold, two forces were applied to the anatomical model hands. We assumed the weight to be equally distributed across both hands and neglected inertial forces and moments. Hand forces were applied at the 2nd knuckle marker position. The computed IK joint angles and box forces were filtered (2nd order Butterworth, cut-off 6 Hz) and used to obtain real-time L5/S1 joint ID moments. Subsequently, IK-derived joint angles, box forces and MTU forces derived from our EMG-driven musculoskeletal model (Section 2.2.3) were transferred to RTOSIM plug-in. RTOSIM plug-in computed joint reaction analyses (JRA), by solving Newton-Euler equations, which included all translational forces and rotational moments for all bodies in the model. Hence, the sum of contact forces between consecutive bodies was computed, resulting in L5/S1 joint compression forces (Fig. 2).

The EMG plug-in managed the TCP/IP streaming of raw data from EMG amplifiers and the processing steps to extract EMG linear envelopes: bandpass filter (30–300 Hz), rectification and low-pass filter (3 Hz). Filtered EMG linear envelopes were normalized using EMG values from isometric maximum contraction recordings. Subsequently, EMG linear envelopes were transferred to the EMG-driven musculoskeletal model block, where they were used as input for the computation of MTU forces (Section 2.2.3).

Table 1
Modifications applied to the lifting full-body model to achieve real-time performance.

Property	LFB	Adapted LFB
Number of bodies	29	17
Number of joints	29	17
Number of degrees of freedom	59	39
Number of muscle tendon units	238	166
Linear coupler constraints	Present	Not present
Weld joints	Sacrum joint	Sacrum, left and right wrist joints

Table 2
Muscle-tendon unit groups in the adapted lifting full-body model and associated measured bipolar electromyograms (EMG). Muscle-tendon units belonging to latissimus dorsi, multifidus, quadratus lumborum and psoas major muscle groups were not driven by EMGs, therefore, solely contributing with the passive musculotendon force component.

Muscle group in adapted lifting-full body model	Measured EMG
Rectus abdominis, external and internal obliques	Rectus abdominis
Iliocostalis pars lumborum	Iliocostalis
Longissimus thoracis pars lumborum	Longissimus thoracis pars lumborum
Longissimus thoracis pars thoracis and iliocostalis pars thoracis	Longissimus thoracis pars thoracis

2.2.3. Real-time EMG-driven musculoskeletal modelling

Our real-time EMG-driven musculoskeletal trunk model relied on the anatomical model described in Section 2.2.1. Model musculotendon forces were estimated using IK-derived L5/S1 joint kinematics and experimentally measured trunk EMGs.

EMG-driven model calibration. First, a mapping between measured EMGs and their associated model MTUs was established (Table 2). As we utilized surface bipolar EMG, we were unable to measure the activity of deep muscles (psoas major, quadratus lumborum and multifidus), for which we only computed the passive force component. Then, subject-specific EMG-driven models were calibrated by tuning MTU maximum isometric force, tendon-slack length, optimal fibre length and EMG shape factor. For this, a simulated annealing algorithm (Goffe et al., 1994) utilized measured EMGs and spline-derived MTU lengths and moment arms, to minimize the difference between reference ID and EMG-based L5/S1 moments. The calibration procedure included one lifting repetition for each experimental condition (Section 2.3).

EMG-driven model execution. Calibrated EMG-driven models received EMG linear envelopes from the EMG plug-in, and these were transformed by accounting for the linear or non-linear EMG-force relationship (Buchanan et al., 2004), as follows:

$$a(t) = \frac{e^{Au(t)} - 1}{e^{A} - 1} \quad (1)$$

where $a(t)$ are the resulting MTU activations, A the non-linear shape factor (constrained to $-3 < A < 0$, with 0 being a linear relationship) and $e(t)$ the filtered EMG linear envelopes.

Hill-type muscle models were used to represent muscle–tendon fibres, which included an active contractile element in parallel with a passive element and a linear damper, as well as a representation of a stiff tendon (Sartori et al., 2012b). Therefore, muscle fibres were modelled using force-velocity, passive and active force-length curves. MTU forces were computed in real-time as a function of MTU activation, length, fibre contraction velocity and pennation angle. Subsequently, estimated MTU forces were used altogether with spline-derived MTU moment arms to estimate L5/S1 joint flexion-extension moments (will be referred as NMS moments). Lastly, the estimated MTU forces were transferred to RTOSIM plug-in to perform JRA (via OpenSim API), obtaining lumbosacral joint compression forces.

Electromechanical delay. During model execution, our real-time pipeline did not include a time-delay compensating for the electromechanical delay (time difference between EMG and force production), leading to NMS moments out-of-phase relative to ID moments (Lloyd et al., 2003). To estimate and compensate for the electromechanical delay, cross-correlations analyses between ID and NMS moments were conducted (Van Dieën et al., 1991). Subsequently, real-time L5/S1 NMS moments and compression forces were time-shifted accordingly to compensate for this delay.

Nevertheless, in the EMG-model calibration stage, our developed algorithm implemented an 80 ms time-delay (based on prior testing) for EMG recordings, which simulated the muscle electromechanical delay, therefore, improving calibration outcomes.

2.3. Experimental protocol

The experimental protocol was divided into calibration and experiment sessions. In both, after marker and electrode placement and maximum voluntary contraction recordings, participants performed symmetric box-lifting tasks (width x depth x height: 40 × 30 × 22 cm) using squat (upright trunk and flexed knees) and stoop (flexed trunk and extended but not locked knees) lifting techniques and two weight conditions (5 and 15 kg). Lifting repetitions consisted of (1) bending over to grab the box (which was resting on 28 cm-height platform), (2) lifting the box until upright posture, (3) bending over to place the box and (4) returning to upright posture. To control for movement speed, a metronome (30 beats-per-minute) indicated the start each of the aforementioned phases.

In the calibration session, participants performed one lifting repetition for each of the four lifting conditions. In the experiment session, participants performed box-liftings with (EXO) and without (NOEXO) exoskeleton. For each of the eight experimental conditions, ten lifting repetitions were recorded, including 1-min rests after two liftings. Lifting repetitions were randomized and NOEXO conditions were recorded first.

2.4. Study analyses

The validity of our real-time EMG-driven framework for L5/S1 flexion-extension moment estimation was evaluated by computing the coefficient of determination (R^2) and root mean squared errors (RMSE) between real-time reference ID and NMS L5/S1 moments. Additionally, we quantified the real-time computational performance of our methodology by computing average computation times (via std::chrono:: system_clock class in C++11) for: IK, ID, B-Spline, NMS moment and JRA processing blocks. An additional analysis comparing our real-time model with our previously proposed offline EMG-driven model (Moya-Esteban et al., 2022) can be found in the Supplementary Materials.

2.4.1. Statistical analyses

Mean EMGs, L5/S1 joint angle, NMS moments and compression forces across 10 participants were divided into 8 time-segments (each 12.5% of the lifting cycle, matching half of the movement consisting of going from upright to fully flexed posture, or viceversa). One-tailed paired-samples t-tests compared the integral of EMGs, NMS moments and compression forces between EXO and NOEXO conditions, at each time segment. Two-tailed t-tests checked for differences in L5/S1 angles. Non-parametric permutation tests were conducted whenever normality of residuals (tested via D'Agostino-Pearson tests) was not met. Statistical analyses were performed using the spm1d package in Matlab 2017 (https://www.spm1d.org) and statistical significance was $\alpha = 0.05$.

3. Results

3.1. Real-time model validation

For all participants and NOEXO conditions, the average estimated electromechanical delay was 88.90 ± 15.39 ms. Prior to EMD compensation, real-time NMS moments and reference ID moments are depicted in Fig. 3. The average R^2 across participants and NOEXO conditions was 0.70, which increased by 13% after EMD-compensation (0.79). Similarly, the average $RMSE_{RMS}$ (RMSE normalized to the RMS of reference moments) decreased by 13% (from 0.31 to 0.27) after EMD-compensation (Fig. 4). Similar mean moment peaks were obtained from ID and EMG-model methodologies, finding the highest and lowest agreement in stoop 5 kg (ID: 2.32 ± 0.14 N m/kg; NMS: 2.35 ± 0.37 N m/kg) and squat 5 kg (ID: 2.06 ± 0.27 N m/kg; NMS: 2.34 ± 0.37 N m/kg), respectively.

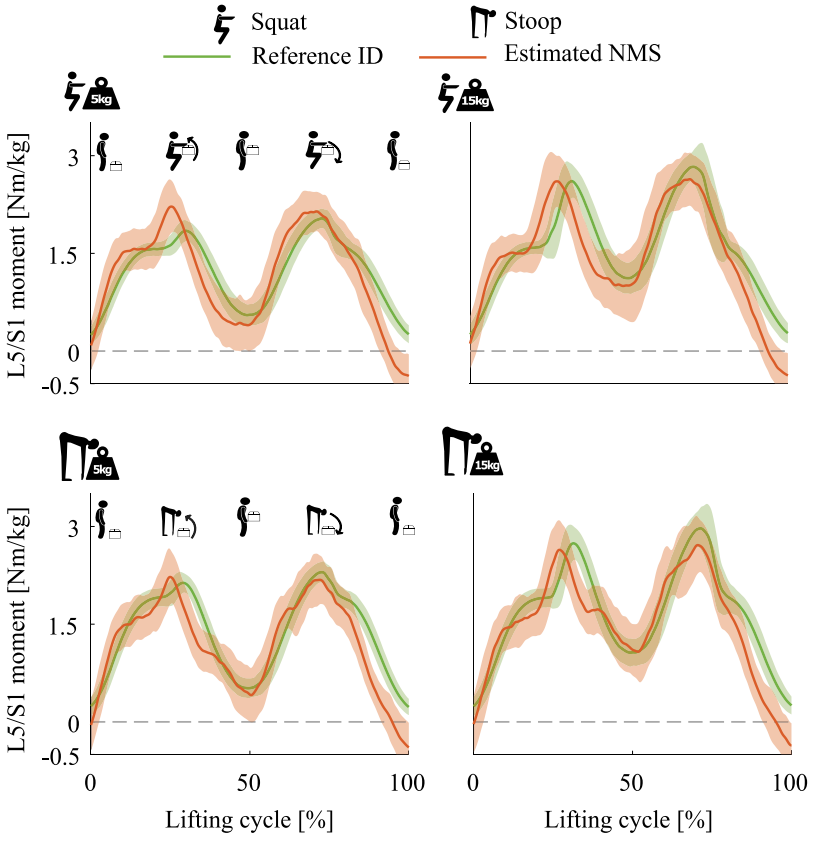

Fig. 3. Real-time inverse dynamics (ID) and EMG-driven musculoskeletal (NMS) L5/S1 joint flexion-extension moments for NOEXO experimental conditions (top row: squat 5 and 15 kg, bottom row: stoop 5 and 15 kg). NMS moments are shown prior to electromechanical delay compensation. Moment values are normalized to participants body weight. Solid lines represent the mean moment across all participants and shaded areas correspond to ± 1 standard deviation. (For interpretation of the references to colour in this figure legend, the reader is referred to the web version of this article.)

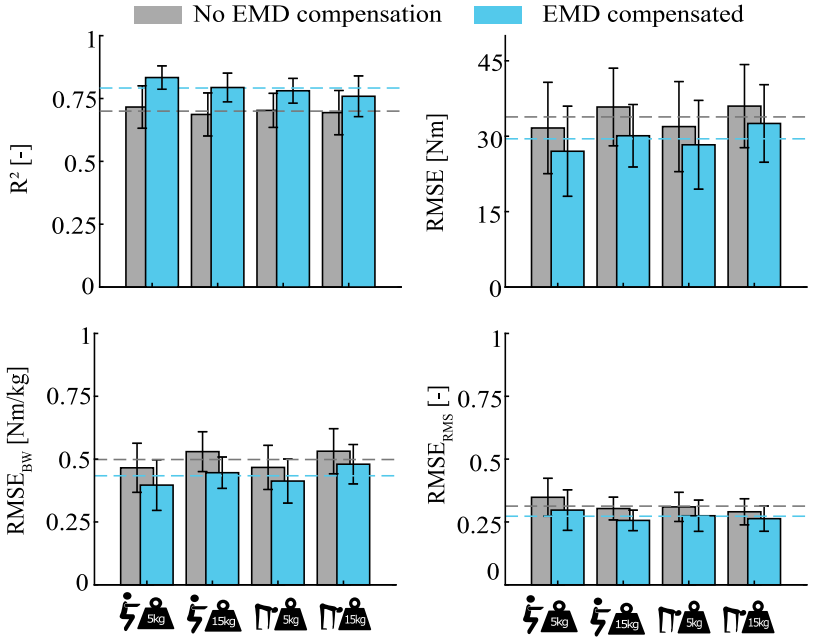

Fig. 4. Coefficient of determination (R^2) and root mean squared errors: absolute (RMSE) normalized to body weight ($RMSE_{BW}$) and normalized with respect to the root mean square of the reference moment ($RMSE_{RMS}$), between real-time inverse dynamics and EMG-driven L5/S1 joint moments. Grey bars correspond to the moment comparison where the electromechanical delay (EMD) was not compensated, while for blue bars, EMD was compensated. Horizontal dashed lines depict the mean values across the four lifting conditions when compensating and not for the EMD in blue and grey, respectively. All R^2 values were statistically significant ($p < 0.05$).

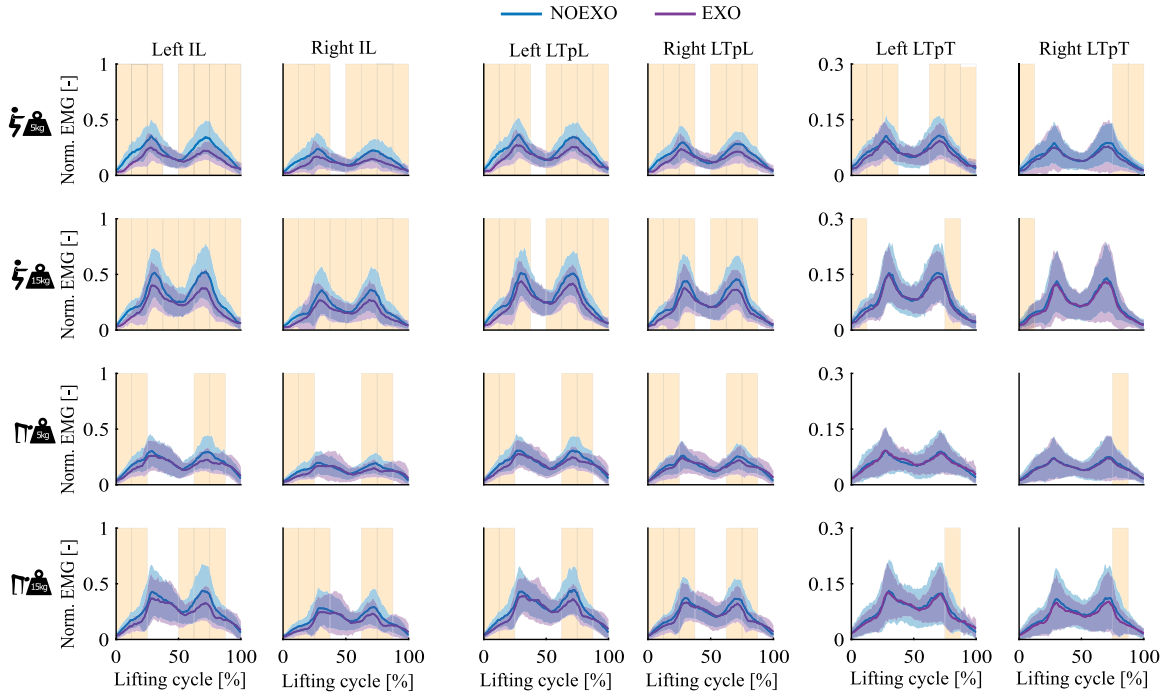

Fig. 5. Normalized electromyography (EMG) activity comparison for all lifting conditions with (EXO) and without (NOEXO) the Laevo Flex exoskeleton, for all recorded thoracolumbar muscles: iliocostalis (IL), longissimus thoracis pars lumborum (LTpL) and longissimus thoracis pars thoracis (LTpT). Rows represent all lifting conditions: squat (5 and 15 kg) and stoop (5 and 15 kg). Solid lines represent the mean normalized EMG across all participants and shaded areas correspond to ± 1 standard deviation. Background orange shaded areas highlight time-segments with statistically significant EMG reduction at EXO conditions ($p < 0.05$). (For interpretation of the references to colour in this figure legend, the reader is referred to the web version of this article.)

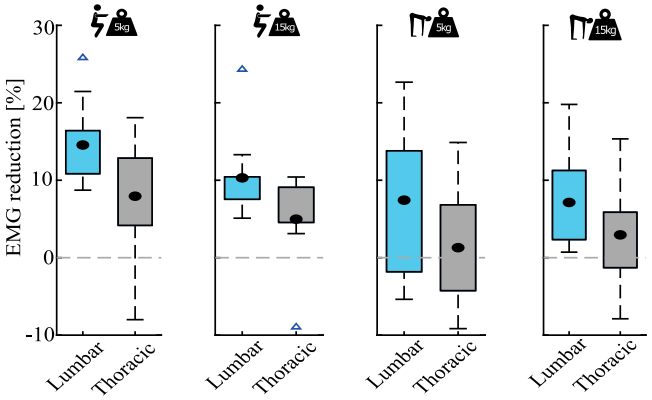

Fig. 6. Mean electromyography (EMG) activity reduction averaged across the complete lifting cycle, for EXO lifting conditions with respect to NOEXO conditions. EMG reduction was computed as the percentage of maximum EMG peaks for each participant and muscle. EMG reductions are shown as the average for lumbar and thoracic muscles. Solid dots and triangles indicate mean values across all participants and outliers, respectively. Data is shown for all lifting techniques (left to right): squat (5 and 15 kg) and stoop (5 and 15 kg).

The average computation time for the major blocks of our real-time modelling pipeline were: IK (24,6 ± 11,1 ms), B-spline (1,7 ± 0,1 ms), NMS moment (0.9 ± 0.1 ms) and joint reaction analysis (54,3 ± 10,1 ms).

3.2. Exoskeleton biomechanical evaluation

For all participants and experimental conditions, the exoskeleton significantly reduced EMG activity for most recorded thoracolumbar muscles (Fig. 5). EMG reduction was mainly present in lumbar musculature (IL and LTpL). For squat lifting, significant EMG reductions were present throughout the whole lifting cycle (except around 50% of the lifting cycle, when participants stood up holding the weight). For the overall squatting cycle, mean EMG activity across participants (expressed as the percentage of maximum EMG peaks) was reduced by 12.4 ± 5.4% and 6.5 ± 6.4% for lumbar and thoracic musculature, respectively (Fig. 6). For stoop lifting, the overall reduction was lower than for squatting (7.3 ± 7.8% and 2.1 ± 7.4% for lumbar and thoracic muscles) and it was mainly present when stooping down to grab the box (0%–25% of the lifting cycle) and when stooping to place the box and going back to upright posture (62.5–87.5% of the lifting cycle).

In specific time-segments of the lifting cycle, L5/S1 joint angles were statistically different between EXO and NOEXO conditions (Fig. 7a). For these time-segments, the maximum angle difference for all experimental conditions was found to be 0.02 radians. For all lifting conditions, L5/S1 NMS moments and compression forces were significantly reduced with respect to NOEXO conditions (Fig. 7a). For the complete lifting cycle and all participants, mean NMS moment reductions were higher for squatting, 17.1 ± 13.9 N m (0.25 ± 0.20 N m/kg; or 9.9 ± 6.7% of the maximum moment peak) than for stooping, 12.0 ± 16.1 N m (0.18 ± 0.24 N m/kg; 6.5 ± 8.2%), see Fig. 7b. A similar trend was observed for L5/S1 compression forces with reductions of 447.5 ± 317.7 N (0.68 ± 0.48 times body weight (xBW); 8.4 ± 5.0%) for squatting, and 310.1 ± 376.8 N (0.47 ± 0.57 xBW; 5.4 ± 6.3%) for stooping (Fig. 7c).

4. Discussion

Real-time technologies monitoring lumbar loading may have a large impact on prevention and treatment of musculoskeletal disorders such as low-back pain, as well as on bio-protective robotic technologies which provide assistance based on spinal forces and aim at maintaining them within safe boundaries. Here, we presented a real-time EMG-driven musculoskeletal model which provides accurate and realistic lumbosacral joint moments and compression forces in line with previous experimental data. Furthermore, we proposed this technology as

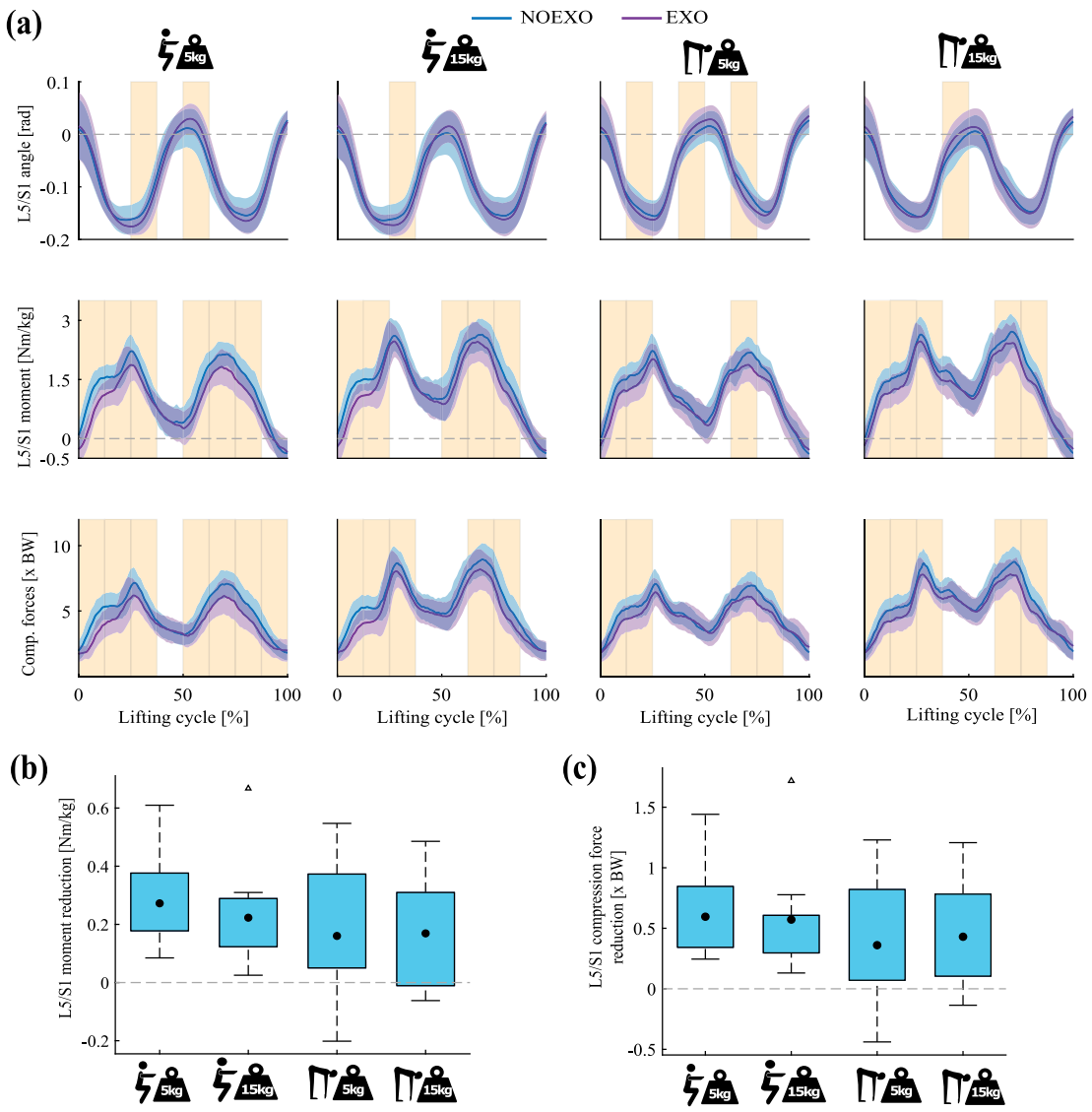

Fig. 7. (a) L5/S1 joint angles, real-time EMG-driven L5/S1 joint moments and real-time compression forces for all lifting conditions with (EXO) and without (NOEXO) the Laevo Flex exoskeleton. Columns represent all lifting conditions: squat (5 and 15 kg) and stoop (5 and 15 kg). Solid lines represent the mean values across all participants and shaded areas correspond to ± 1 standard deviation. Background orange shaded areas highlight time-segments with statistically significant differences in L5/S1 joint angle or significant reduction of L5/S1 joint moment or compression force at EXO conditions ($p < 0.05$). (b) Mean real-time EMG-driven L5/S1 joint moment reduction and (c) real-time L5/S1 joint compression force reduction, averaged across the complete lifting cycle, for EXO lifting conditions with respect to NOEXO conditions. In (b) and (c), solid dots and triangles indicate mean values across all participants and outliers, respectively. (For interpretation of the references to colour in this figure legend, the reader is referred to the web version of this article.)

a robust instrument for biomechanical assessment of back-support exoskeletons aiding lifting tasks. This may enable subject-specific design and real-time personalization of exoskeleton assistance.

Real-time L5/S1 joint moments from our EMG-driven musculoskeletal models were in agreement with reference ID moments, as suggested by correlation values ranging between 0.76–0.83 and average estimation errors, $RMSE_{RMS}$, below 30% of the reference moment for all lifting and weight conditions (Figs. 3 and 4). Previous offline studies based on EMG-driven (Faber et al., 2009; Marras et al., 1999) or inverse dynamics (Schipplein et al., 1990) methodologies have reported similar lumbosacral moment magnitudes, for comparable lifting conditions.

Mean real-time lumbosacral compression forces ranged between 4850–6050 N for stoop 5 kg and squat 15 kg, respectively. A direct validation of these estimates was unfeasible due to the required invasive insertion of sensors. Nonetheless, similar L5/S1 compression forces have been reported in earlier research based on offline EMG-assisted (Ferguson et al., 2002; Koopman et al., 2020b) or static optimization (Kim and Zhang, 2017) approaches. Our estimates displayed similar magnitudes as previous *in vivo* measurements of intradiscal pressures of adjacent lumbar joints. Taking into account intradiscal pressures and the estimated disc area, L4/L5 joint compression force estimates of approximately 5000 N were previously observed for one participant stoop-lifting a 19.8 kg box (Wilke et al., 2001). Additionally, high correlations (R^2 = 0.81) and magnitude differences below 14% were found between L5/S1 compression forces computed with our earlier proposed offline EMG-driven model (Moya-Esteban et al., 2022) and the present real-time pipeline (see Supplementary Materials). This disagreement may stem from differences in implementation of the activation dynamics blocks of the real-time and offline pipelines (Pizzolato et al., 2015), which may have led to different muscle activation, given identical EMGs.

Our modelling pipeline provided real-time estimates of biological joint moments and compression forces, with an average processing delay of 81.5 ms. This time was significantly lower than the previously found electromechanical delay inherent of back musculature (approximately 130 ms; Van Dieën et al., 1991), and the 90 ms estimated

in the present study. This highlights the potential of our framework to become a robust human-machine interface capable of estimating internal biomechanical properties non-invasively and employ them in control actuation strategies of robotic assistive devices as back-support exoskeletons.

Although significant, EMG reductions in this study were lower compared to previous research on back-assistive devices (Lamers et al., 2017; Alemi et al., 2019). In Abdoli-e and Stevenson (2008), EMG activity of the erector spinae muscle was reduced by 24% for similar lifting tasks, when using an elastic-based back-support exoskeleton. Reductions found in the present study were larger during squat than stoop lifting (12.4 and 6.5%, respectively). This may be explained by the fact that during squatting the thigh-torso angle was smaller, therefore, the exoskeleton delivered greater moments to the participants. Our results also highlighted a predominant EMG reduction in the lowering phases of the movement (Fig. 5), suggesting that participants laid their upper-body on the device, relieving therefore the load on back musculature. EMG reductions were also greater for lumbar than thoracic muscles (see Fig. 6), which was expected since the exoskeleton provided assistance at hip level.

We found lumbosacral moments and compression forces to be reduced by 11.9–18.7 N m (6%–12%) and 300–450 N (5%–10%) respectively, which is in agreement with the provided hip assistance (van Harmelen et al., 2022). Previous studies showed similar L5/S1 compression forces reductions (8%–9%) for the previous version of the Laevo exoskeleton (Koopman et al., 2020a) as well as, larger reductions (13%–24%) for active back-support exoskeletons (Koopman et al., 2020b). Although our compression force reductions were slightly lower than previous research, 300–450 N reductions may avoid exceeding previously proposed maximum acceptable lumbar forces (Jäger, 2018), resulting in low-back pain risk reduction. Moreover, participants only followed a short familiarization period with the device. Dedicated training sessions would likely promote an optimal use of the device and improve results at EMG, moment and compression force levels (Diamond-Ouellette et al., 2022).

A limitation of our experiment was the low sampling frequency in kinematic recordings, which may hamper accurate estimations during faster movements. The multiple musculotendon units in our anatomical model and their associated wrapping surfaces around spinal vertebrae, required highly expensive computations in the OpenSim joint reaction tool (Seth et al., 2011), making our pipeline unsuitable for higher sampling frequencies. In future research, a multithreaded implementation will allow for simultaneous computations of multiple JRA frames. Furthermore, lack of randomization of exoskeleton conditions constitutes another limitation of this study. However, this did not likely influence our results since muscle fatigue was minimized with rest periods in between liftings. Additionally, neglecting box-derived inertial forces may have resulted in estimation errors for inverse dynamic moments. The impact of these errors may be reduced due to the slow lifting movements in our protocol.

Another limitation of the present study was the low amount of sampling sites used to measure EMG activity of trunk muscles. First, we did not measure EMG activity of deep trunk muscles such as multifidus, quadratus lumborum or psoas major. Nevertheless, previous research suggests that recording muscle activity of deeper muscles does not result in better muscle forces and spinal force computation (Staudenmann et al., 2005; Van Dieen and Kingma, 2005). Furthermore, unlike our previous offline EMG-driven methodology, we did not record muscle activity from external and internal oblique muscles. Instead, rectus abdominis activity was used to drive all abdominal MTU in our model. The impact of this assumption on our estimates may be reduced as a result of the high co-activity of abdominal musculature during symmetric lifting tasks (Zetterberg et al., 1987).

We presented a real-time EMG-driven musculoskeletal modelling framework capable of estimating accurate lumbosacral joint moments and plausible compression forces, across varied box-lifting conditions. Thanks the calibration stage, our models estimated lumbosacral moments without *a priori* information of the lifted object. This suggests the possibility of applying our framework in out-of-the-lab scenarios where wearable sensors as inertial measurements units and zero-wire EMGs can be used to provide real-time biofeedback on lumbar moments. This technology also demonstrated the capacity of detecting the biomechanical effects on joint loading of assistive devices such as back-support exoskeletons. The proposed framework lays the foundation for the development of devices aiming at providing biofeedback for prevention and treatment of musculoskeletal injury-related disorders. Additionally, this technology presents the potential to develop versatile and adaptive human-machine interfaces for bioprotective robotic devices relying on musculoskeletal variables.

CRediT authorship contribution statement

A. Moya-Esteban: Writing – review & editing, Writing – original draft, Visualization, Validation, Software, Methodology, Investigation, Formal analysis, Data curation, Conceptualization. **G. Durandau:** Writing – review & editing, Supervision, Software, Methodology. **H. van der Kooij:** Writing – review & editing, Supervision, Project administration, Funding acquisition, Conceptualization. **M. Sartori:** Writing – review & editing, Supervision, Project administration, Investigation, Funding acquisition, Conceptualization.

Declaration of competing interest

The authors declare that they have no competing and/or financial interests that could have appeared to influence the work reported in this paper.

Acknowledgements

This work is part of the research program Wearable Robotics with project number P16-05, partly funded by the Dutch Research Council (NWO). Also, the work is supported by the European Research Council (ERC) under the European Union's Horizon 2020 research and innovation program, as part of the ERC Starting, The Netherlands Grant INTERACT (Grant No. 803035), and SOPHIA, The Netherlands project (Grant No. 871237) and by the Interreg North Sea Region, The Netherlands (Exskallerate project).

Appendix A. Supplementary data

Supplementary material related to this article can be found online at https://doi.org/10.1016/j.jbiomech.2023.111727.

References

Abdoli-e, M., Stevenson, J.M., 2008. The effect of on-body lift assistive device on the lumbar 3D dynamic moments and EMG during asymmetric freestyle lifting. Clin. Biomech. 23 (3), 372–380.

Alemi, M.M., Geissinger, J., Simon, A.A., Chang, S.E., Asbeck, A.T., 2019. A passive exoskeleton reduces peak and mean EMG during symmetric and asymmetric lifting. J. Electromyogr. Kinesiol. 47, 25–34.

Bassani, T., Stucovitz, E., Qian, Z., Briguglio, M., Galbusera, F., 2017. Validation of the AnyBody full body musculoskeletal model in computing lumbar spine loads at L4L5 level. J. Biomech. 58, 89–96.

Bazrgari, B., Shirazi-Adl, A., Arjmand, N., 2007. Analysis of squat and stoop dynamic liftings: muscle forces and internal spinal loads. Eur. Spine J. 16 (5), 687–699.

Beaucage-Gauvreau, E., Robertson, W.S., Brandon, S.C., Fraser, R., Freeman, B.J., Graham, R.B., Thewlis, D., Jones, C.F., 2019. Validation of an OpenSim full-body model with detailed lumbar spine for estimating lower lumbar spine loads during symmetric and asymmetric lifting tasks. Comput. Methods Biomech. Biomed. Eng. 22 (5), 451–464.

Boocock, M., Naudé, Y., Taylor, S., Kilby, J., Mawston, G., 2019. Influencing lumbar posture through real-time biofeedback and its effects on the kinematics and kinetics of a repetitive lifting task. Gait Posture 73, 93–100.

Brinckmann, P., Johannleweling, N., Hilweg, D., Biggemann, M., 1987. Fatigue fracture of human lumbar vertebrae. Clin. Biomech. 2 (2), 94–96.

Buchanan, T.S., Lloyd, D.G., Manal, K., Besier, T.F., 2004. Neuromusculoskeletal modeling: estimation of muscle forces and joint moments and movements from measurements of neural command. J. Appl. Biomech. 20 (4), 367.

Delp, S.L., Anderson, F.C., Arnold, A.S., Loan, P., Habib, A., John, C.T., Guendelman, E., Thelen, D.G., 2007. OpenSim: open-source software to create and analyze dynamic simulations of movement. IEEE Trans. Biomed. Eng. 54 (11), 1940–1950.

Diamond-Ouellette, G., Telonio, A., Karakolis, T., Leblond, J., Bouyer, L., Best, K., 2022. Exploring the change in metabolic cost of walking before and after familiarization with a passive load-bearing exoskeleton: A case series. IISE Trans. Occup. Ergon. Hum. Factors 10 (3), 161–172.

Dreischarf, M., Shirazi-Adl, A., Arjmand, N., Rohlmann, A., Schmidt, H., 2016. Estimation of loads on human lumbar spine: A review of in vivo and computational model studies. J. Biomech. 49 (6), 833–845.

Durandau, G., Farina, D., Sartori, M., 2017. Robust real-time musculoskeletal modeling driven by electromyograms. IEEE Trans. Biomed. Eng. 65 (3), 556–564.

Durandau, G., Rampeltshammer, W.F., van der Kooij, H., Sartori, M., 2022. Neuromechanical model-based adaptive control of bilateral ankle exoskeletons: Biological joint torque and electromyogram reduction across walking conditions. IEEE Trans. Robot..

El Ouaaid, Z., Shirazi-Adl, A., Arjmand, N., Plamondon, A., 2013. Coupled objective function to study the role of abdominal muscle forces in lifting using the kinematics-driven model. Comput. Methods Biomech. Biomed. Eng. 16 (1), 54–65.

Faber, G.S., Kingma, I., Bakker, A.J., Van Dieën, J.H., 2009. Low-back loading in lifting two loads beside the body compared to lifting one load in front of the body. J. Biomech. 42 (1), 35–41.

Ferguson, S., Gaudes-MacLaren, L., Marras, W., Waters, T., Davis, K., 2002. Spinal loading when lifting from industrial storage bins. Ergonomics 45 (6), 399–414.

Fortini, L., Lorenzini, M., Kim, W., De Momi, E., Ajoudani, A., 2020. A real-time tool for human ergonomics assessment based on joint compressive forces. In: 2020 29th IEEE International Conference on Robot and Human Interactive Communication (RO-MAN). IEEE, pp. 1164–1170.

Freburger, J.K., Holmes, G.M., Agans, R.P., Jackman, A.M., Darter, J.D., Wallace, A.S., Castel, L.D., Kalsbeek, W.D., Carey, T.S., 2009. The rising prevalence of chronic low back pain. Arch. Intern. Med. 169 (3), 251–258.

Goffe, W.L., Ferrier, G.D., Rogers, J., 1994. Global optimization of statistical functions with simulated annealing. J. Econometrics 60 (1–2), 65–99.

van Harmelen, V., Schnieders, J., Wagemaker, S., 2022. Measuring the amount of support of lower back exoskeletons.

Hensel, R., Keil, M., 2019. Subjective evaluation of a passive industrial exoskeleton for lower-back support: A field study in the automotive sector. IISE Trans. Occup. Ergon. Hum. Factors 7 (3–4), 213–221.

Hughes, R.E., Chaffin, D.B., Lavender, S.A., Andersson, G.B., 1994. Evaluation of muscle force prediction models of the lumbar trunk using surface electromyography. J. Orthop. Res. 12 (5), 689–698.

Jäger, M., 2018. Extended compilation of autopsy-material measurements on lumbar ultimate compressive strength for deriving reference values in ergonomic work design: The Revised Dortmund Recommendations. EXCLI J. 17, 362.

Kim, H.-K., Zhang, Y., 2017. Estimation of lumbar spinal loading and trunk muscle forces during asymmetric lifting tasks: application of whole-body musculoskeletal modelling in OpenSim. Ergonomics 60 (4), 563–576.

Koopman, A.S., Kingma, I., de Looze, M.P., van Dieën, J.H., 2020a. Effects of a passive back exoskeleton on the mechanical loading of the low-back during symmetric lifting. J. Biomech. 102, 109486.

Koopman, A.S., Näf, M., Baltrusch, S.J., Kingma, I., Rodriguez-Guerrero, C., Babič, J., de Looze, M.P., van Dieën, J.H., 2020b. Biomechanical evaluation of a new passive back support exoskeleton. J. Biomech. 105, 109795.

Lamers, E.P., Yang, A., Zelik, K.E., 2017. Biomechanically-assistive garment offloads low back during leaning and lifting. In: Proc. 41st Annu. Meeting of the American Society of Biomechanics.

Lloyd, D., Littlewood, J., Craig, M., Thomsett, L., 2003. Practical Equine Dermatology. SF 959. S54. P72 2003. Wiley Online Library.

Lorenzini, M., Kim, W., Ajoudani, A., 2022. An online multi-index approach to human ergonomics assessment in the workplace. IEEE Trans. Hum.-Mach. Syst..

Lotti, N., Xiloyannis, M., Durandau, G., Galofaro, E., Sanguineti, V., Masia, L., Sartori, M., 2020. Adaptive model-based myoelectric control for a soft wearable arm exosuit: A new generation of wearable robot control. IEEE Robot. Autom. Mag. 27 (1), 43–53.

Lu, Z., Chen, X., Zhang, X., Tong, K.-Y., Zhou, P., 2017. Real-time control of an exoskeleton hand robot with myoelectric pattern recognition. Int. J. Neural Syst. 27 (05), 1750009.

Manal, K., Gravare-Silbernagel, K., Buchanan, T.S., 2012. A real-time EMG-driven musculoskeletal model of the ankle. Multibody Syst. Dyn. 28 (1), 169–180.

Marras, W., Granata, K., Davis, K., Allread, W., Jorgensen, M., 1999. Effects of box features on spine loading during warehouse order selecting. Ergonomics 42 (7), 980–996.

Moya-Esteban, A., Brouwer, N.P., Tabasi, A., Van Der Kooij, H., Kingma, I., Sartori, M., 2020. Muscle-level analysis of trunk mechanics via musculoskeletal modeling and high-density electromyograms. In: 2020 8th IEEE RAS/EMBS International Conference for Biomedical Robotics and Biomechatronics (BioRob). IEEE, pp. 1109–1114.

Moya-Esteban, A., van der Kooij, H., Sartori, M., 2022. Robust estimation of lumbar joint forces in symmetric and asymmetric lifting tasks via large-scale electromyography-driven musculoskeletal models. J. Biomech. 111307.

Nachemson, A., Morris, J.M., 1964. In vivo measurements of intradiscal pressure: discometry, a method for the determination of pressure in the lower lumbar discs. JBJS 46 (5), 1077–1092.

Ning, X., Zhou, J., Dai, B., Jaridi, M., 2014. The assessment of material handling strategies in dealing with sudden loading: The effects of load handling position on trunk biomechanics. Applied Ergon. 45 (6), 1399–1405.

Norman, R., Wells, R., Neumann, P., Frank, J., Shannon, H., Kerr, M., 1998. A comparison of peak vs cumulative physical work exposure risk factors for the reporting of low back pain in the automotive industry. Clin. Biomech. 13 (8), 561–573.

Peters, S., Tabasi, A., Kingma, I., van Dijk, W., van Dieën, J.H., 2022. Development of a real time estimation method of L5S1 moments in occupational lifting. J. Biomech. 111417.

Pizzolato, C., Lloyd, D.G., Sartori, M., Ceseracciu, E., Besier, T.F., Fregly, B.J., Reggiani, M., 2015. CEINMS: A toolbox to investigate the influence of different neural control solutions on the prediction of muscle excitation and joint moments during dynamic motor tasks. J. Biomech. 48 (14), 3929–3936.

Pizzolato, C., Reggiani, M., Modenese, L., Lloyd, D., 2017a. Real-time inverse kinematics and inverse dynamics for lower limb applications using OpenSim. Comput. Methods Biomech. Biomed. Eng. 20 (4), 436–445.

Pizzolato, C., Reggiani, M., Saxby, D.J., Ceseracciu, E., Modenese, L., Lloyd, D.G., 2017b. Biofeedback for gait retraining based on real-time estimation of tibiofemoral joint contact forces. IEEE Trans. Neural Syst. Rehabil. Eng. 25 (9), 1612–1621.

Rohlmann, A., Bergmann, G., Graichen, F., 1999. Loads on internal spinal fixators measured in different body positions. Eur. Spine J. 8 (5), 354–359.

Rohlmann, A., Dreischarf, M., Zander, T., Graichen, F., Strube, P., Schmidt, H., Bergmann, G., 2013. Monitoring the load on a telemeterised vertebral body replacement for a period of up to 65 months. Eur. Spine J. 22 (11), 2575–2581.

Samy, V., Ayusawa, K., Yoshida, E., 2019. Real-time musculoskeletal visualization of muscle tension and joint reaction forces. In: 2019 IEEE/SICE International Symposium on System Integration. SII, IEEE, pp. 396–400.

Sartori, M., Durandau, G., Došen, S., Farina, D., 2018. Robust simultaneous myoelectric control of multiple degrees of freedom in wrist-hand prostheses by real-time neuromusculoskeletal modeling. J. Neural Eng. 15 (6), 066026.

Sartori, M., Reggiani, M., van den Bogert, A.J., Lloyd, D.G., 2012a. Estimation of musculotendon kinematics in large musculoskeletal models using multidimensional B-splines. J. Biomech. 45 (3), 595–601.

Sartori, M., Reggiani, M., Farina, D., Lloyd, D.G., 2012b. EMG-driven forward-dynamic estimation of muscle force and joint moment about multiple degrees of freedom in the human lower extremity. PLoS One 7 (12), e52618.

Schipplein, O., Trafimow, J., Andersson, G., Andriacchi, T., 1990. Relationship between moments at the L5/S1 level, hip and knee joint when lifting. J. Biomech. 23 (9), 907–912.

Schultz, A., Andersson, G., Ortengren, R., Haderspeck, K., Nachemson, A., 1982. Loads on the lumbar spine. Validation of a biomechanical analysis by measurements of intradiscal pressures and myoelectric signals. J. Bone Joint Surg. Am. Vol. 64 (5), 713–720.

Seth, A., Sherman, M., Reinbolt, J.A., Delp, S.L., 2011. OpenSim: a musculoskeletal modeling and simulation framework for in silico investigations and exchange. Procedia Iutam 2, 212–232.

Settembre, N., Maurice, P., Paysant, J., Theurel, J., Claudon, L., Kimmoun, A., Levy, B., Hani, H., Chenuel, B., Ivaldi, S., 2020. The use of exoskeletons to help with prone positioning in the intensive care unit during COVID-19. Ann. Phys. Rehabil. Med. 63 (4), 379–382.

Sherman, M.A., Seth, A., Delp, S.L., 2011. Simbody: multibody dynamics for biomedical research. Procedia Iutam 2, 241–261.

Staudenmann, D., Kingma, I., Stegeman, D.F., van Dieën, J.H., 2005. Towards optimal multi-channel EMG electrode configurations in muscle force estimation: a high density EMG study. J. Electromyogr. Kinesiol. 15 (1), 1–11.

Van Dieen, J., Kingma, I., 2005. Effects of antagonistic co-contraction on differences between electromyography based and optimization based estimates of spinal forces. Ergonomics 48 (4), 411–426.

Van Dieën, J., Thissen, C., Van de Ven, A., Toussaint, H., 1991. The electro-mechanical delay of the erector spinae muscle: influence of rate of force development, fatigue and electrode location. Eur. J. Appl. Physiol. Occup. Physiol. 63 (3), 216–222.

Ventura, L., Lorenzini, M., Kim, W., Ajoudani, A., 2021. A flexible robotics-inspired computational model of compressive loading on the human spine. IEEE Robot. Autom. Lett. 6 (4), 8229–8236.

Wilke, H.-J., Neef, P., Hinz, B., Seidel, H., Claes, L., 2001. Intradiscal pressure together with anthropometric data–a data set for the validation of models. Clin. Biomech. 16, S111–S126.

Zetterberg, C., Andersson, G., Schultz, A.B., 1987. The activity of individual trunk muscles during heavy physical loading. Spine 12 (10), 1035–1040.